Focusing of baroclinic tidal energy in a canyon

Vlasenko, Vasiliy; Stashchuk, Nataliya; Inall, Mark; Porter, Marie; Aleynik, Dmitry

Published in:
Journal of Geophysical Research
Publication date:
2016

Focusing of baroclinic tidal energy in a canyon

Vasiliy Vlasenko,[1] Nataliya Stashchuk,[1] Mark E. Inall,[2] Marie Porter,[2] and Dmitry Aleynik[2]

Corresponding author: V. VLasenko, School of Marine Science and Engineering, University of Plymouth, Drake Circus, Plymouth, PL4 8AA, UK. (vvlasenko@plymouth.ac.uk)

[1]School of Marine Science and Engineering, University of Plymouth, UK.

[2]Scottish Association for Marine Science, Scottish Marine Institute, Oban, UK.

Abstract.

Strong three dimensional focusing of internal tidal energy in the Petite Sole Canyon in the Celtic Sea is analysed using observational data and numerical modelling. In a deep layer (500-800m) in the centre of the canyon shear variance was elevated by an order of magnitude. Corresponding large vertical oscillations of deep isotherms, and a local maximum of horizontal velocity were replicated numerically using the MITgcm. The elevated internal tidal activity in the deep part of the canyon is explained in terms of the downward propagation and focusing of multiple internal tidal beams generated at the shelf break. The near-circular shape of the canyon head and steep bottom topography throughout the canyon (steeper than the tidal beam) create favourable conditions for the lens-like focusing of tidal energy in the canyon's centre. Observations and modeling show that the energy focusing greatly intensifies local diapycnal mixing, that leads to local formation of a baroclinic eddy.

1. Introduction

Oceanic canyons are potential places for significant tidal energy conversion from the barotropic to baroclinic modes, with major implications for water mass mixing. According to *Hickey* [1995], nearly 20% of the shelf edge between Alaska and the equator is dominated by steep, narrow, and abrupt canyons. Historically, the first and most extensively studied canyon was La Jolla Canyon (California). The results by *Shepard* [1974] and *Gordon and Marshall* [1976] showed that steep canyons can act as a trap for tidally generated internal waves. Specifically, it was recognised that the dynamical processes occurring in canyons strongly depend on the ratio of the maximum bottom steepness ($S_{topo} = \partial H/\partial l$) (here $H(x, y)$ is the water depth, and l is the direction of the maximum bottom gradient) to the inclination of the characteristic paths of the internal wave energy propagation

$$S_{wave} = dz/dl = \pm[(\omega^2 - f^2)/(N^2(z) - \omega^2)]^{1/2} \quad (1)$$

where ω is the tidal frequency, f is the Coriolis parameter, and $N(z)$ is the buoyancy frequency. In other words, in terms of the mechanism of internal wave dynamics, the following parameter

$$\alpha(x, y, z) = \frac{S_{topo}}{S_{wave}} = \frac{|\partial H/\partial l|}{[(\omega^2 - f^2)/(N^2(z) - \omega^2)]^{1/2}} \quad (2)$$

is the principal measure of the bottom steepness that distinguishes two very different regimes of tidal energy conversion. Schematically they are presented in Figure 1. For specificity, the buoyancy frequency measured in a canyon of the Celtic Sea (reported in [*Vlasenko and Stashchuk*, 2015]) is used for the analysis, see Figure 1 a.

In a subcritical regime, when the condition $\alpha < 1$ is valid over the whole domain, it is mostly the lower tidal baroclinic modes that are generated. This regime is presented in Figure 1 b.

Over "steep" topographies, for which $\alpha > 1$ occurs at least for some fragments of a given slope, the supercritical regime of tidal energy conversion, presented in Figure 1 c (below point C), is fulfilled. In this regime internal tidal energy is concentrated in a narrow internal tidal beam (magenta stripe in Figure 1 c) that radiates energy away from bottom fragments where $\alpha = 1$. The energy propagates in the tidal beam upward and downward along characteristic line (1) with group velocity C_g while the wave phase propagates across the beam with the phase speed C_p, Figure 1 c. In fact, it is not only the point C with $\alpha = 1$ is the place of the beam formation. A wider area A-B where the bottom inclination is close to critical is the place of the beam generation. More on different regimes of tidal energy conversion can be found in *Vlasenko et al.* [2005]).

Note that the tidal beam is a superposition of many baroclinic modes, and the presence of a beam is evidence of higher mode excitation. For a typical "V"-shaped canyon with $\alpha \geq 1$ the baroclinic tidal energy is trapped inside the canyon, being able only to propagate downward reflecting many times from canyon's steep flanks without any opportunity of escape.

The importance of the relative bottom steepness α for internal wave dynamics in canyons was acknowledged by *Petruncio et al.* [1998] in their interpretation of measurements conducted in another well-studied canyon, - Monterey Submarine Canyon. Note, however, that in further analyses (for example *Zhao et al.* [2012]) the focus was predominantly on

the investigation of the energetic characteristics of internal waves and turbulent mixing without proper reference to the topographic steepness.

Some studies on the baroclinic dynamics in canyons were conducted for an idealized bottom profile by *Baines* [1983]; *Grimshaw et al.* [1985]. A more realistic model set up, specifically, the real bottom topography, was taken in a further series of numerical experiments performed for Monterey Submarine Canyon area: *Petruncio et al.* [2002] used POM, *Jachec et al.* [2006] operated with SUNTANS, and *Hall and Carter* [2011] used POM to investigate internal tides in the canyon area. However, the specific role of the relative steepness α of the canyon topography in the distribution of the baroclinic wave energy was not investigated in any of these studies. Specifically, the structure of the baroclinic tidal field in the areas where $\alpha > 1$, a common occurrence, has not hitherto been discussed in detail.

The purpose of this paper is to interpret the three-dimensional effects of internal tidal dynamics that are seen to occur in supercritical canyons. In particular, an original observational data set collected in a supercritical canyon in the Celtic Sea is analysed here in terms of the focusing of internal tidal energy radiated from the areas with critical bottom inclination.

2. Observations

The Celtic Sea is a 200 meter deep, wide shelf sea with a large number of headlands and canyons along its shelf edge, Figure 2 a. Observations analysed here were conducted on the 376-th cruise of the RRS "Discovery" (hereafter D376) in June 2012, as part of the FASTNEt study to quantify the cross shelf transport on the NE Atlantic Ocean margin. With relevance to this paper, 14 repeat "yo-yo" CTD profiles were conducted at a station

precisely in the middle of the Petite Sole Canyon presented in Figure 2 b. Vertical profiles were repeated with approximately one hour time interval to the depth of approximately 1000 m. In addition to the CTD probe, a downward looking TRDI WHM 300kHz LADCP was mounted on the frame, so that each CTD profile was accompanied by a vertical profile of currents.

All 14 "yo-yo" temperature profiles $T_j(z)$ ($j = 1, 2, 3, \ldots, 14$) are presented in Figure 3 a by blue lines. The red line shows an equilibrium temperature distribution calculated as an average temperature at each depth. Comparing all individual temperature profiles $T_j(z)$ with the average $T(z)$ one can see that the largest deviations of every individual profile from the average take place in two zones: in the surface 150 m layer, and between 500 m and 900 m depth. Assuming that these deviations were caused by the dynamical processes developing in the canyon, the vertical displacement ζ_j of every individual isotherm on every profile from its equilibrium state (which the averaged temperature profile represents) can be calculated using the following formula:

$$\zeta_j = \frac{|T_j - T|}{\partial T/\partial z}$$

An average profile of isotherms displacements, calculated as $1/14\sum_{j=1}^{14}\zeta_j(z)$, is presented in Figure 3 b. It shows that the maximum vertical displacements of isotherms, up to 45 m, are located in deep water, between 600 and 800 m depth.

Note that the maximum baroclinic horizontal velocities at the "yo-yo" station were, as expected, recorded by the LADCP in the surface layer. However, Figure 3 b suggests that a comparable contribution of the 600-800 m depth layer to the internal wave energy is also expected. In order to quantify the kinetic energy of dynamical processes developing at the "yo-yo" station, an average profile of horizontal velocities for all 14 LADCP sampling

was calculated as follows

$$U(z) = 1/14 \sum_{j=1}^{14} \sqrt{u_j^2(z) + v_j^2(z)}.$$

Here $u_j(z)$ and $v_j(z)$ $(j = 1, 2, \ldots, 14)$ are eastward and northward velocities.

The mean profile of $U(z)$ is presented in Figure 3 c (magenta line). It shows the velocity maximum at the free surface as well as a secondary local maxima at the depth of 680 m which coincides with the position the maximum vertical displacement and a broad region of of elevated currents between 600 m and 800 m, produced presumably by the action of internal waves.

As a proxy-measure for the relative strength of diapycnal mixing, we follow the method of *Polzin et al.* [2002] in computing the buoyancy-normalised LADCP shear in overlapping segments (50% overlap), each of 128 meters in vertical extent. The spectra for each segment were then integrated between vertical wavelengths of 25 m to 128 m, to give 14 profiles of shear variance, a property that scales with the diapycnal eddy diffusivity. The time averaged vertical profile of the shear variance (Figure 3 d) demonstrates a relative 7-fold increase below 700 m depth, with a broad maximum at 780 m. The necessary segmentation of the data results in loss of vertical resolution in comparison with temperature or velocity profiles, but nevertheless a consistent deep maximum in fine-structure derived vertical mixing is clearly apparent.

In order to bring more clarity to the interpretation of these relatively sparse observations and to understand the reasons for apparent internal wave energy and vertical mixing intensification in the deep part of the canyon, a series of numerical experiments was conducted.

3. Modelling

The fully non-linear non-hydrostatic MITgcm was used to model internal tides in the canyon and the surrounding area (see Figure 2 b). In the main part of the model domain the horizontal and vertical resolutions were 100 m and 10 m, respectively. In order to avoid any spurious boundary reflections, an exponentially increasing horizontal grid step near the lateral boundaries was used that guaranteed an accurate numerical solution within the internal model domain without any signals reflected from the boundaries during at least 10 tidal cycles.

The tidal forcing was set in the model by a tidal potential added to the right hand side of the momentum balance equations. Its intensity was chosen using [*Egbert and Erofeeva*, 2002] in such a way as to reproduce tidal velocities recorded by moored ADCP current meters deployed during D376. Spatial distribution of tidal ellipses is shown in Figure 2 d. A vertical stratification was introduced into the model after setting the tidal forcing for a homogeneous fluid. The temperature and salinity profiles were taken from the direct CTD measurements at the yo-yo station.

The Richardson number dependent parameterisation for vertical viscosity ν and diffusivity κ introduced in [*Pacanowski and Philander*, 1981] was used:

$$\nu = \frac{\nu_0}{(1+\alpha \mathrm{Ri})^n} + \nu_b, \quad \kappa = \frac{\nu}{(1+\alpha \mathrm{Ri})} + \kappa_b.$$

Here Ri is the Richardson number, $\mathrm{Ri} = N^2(z)/(u_z^2 + v_z^2)$, u and v are the components of horizontal velocity; $N(z)$ is the buoyancy frequency $N^2(z) = -g/\rho(\partial\rho/\partial z)$ in which g is the acceleration due to gravity and ρ is the water density; ν_b=10^{-5} m^2 s^{-1} and κ_b=10^{-5} m^2 s^{-1} are the background viscosity, and diffusivity, respectively; ν_0=$1.5{\cdot}10^{-2}$ m^2 s^{-1}, α=5 and n=1 are the adjustable parameters. Such a parametrisation increases ν and κ in

areas where the Richardson number is small. The horizontal viscosity and diffusivity were set to a constant value of $0.5\,\mathrm{m^2\,s^{-1}}$. More details on the model initialization and input parameters can be found in *Vlasenko et al.* [2014].

The model was forced by M_2 tidal harmonic which is predominant in the area (*Egbert and Erofeeva* [2002]). The principal question to be addressed by the modelling efforts is to identify the cause of the highly energetic internal wave activity in the centre of the canyon below 500 m depth. The modelling evidence of this intensification in deep water is seen in Figure 4 where the amplitude of the model-predicted horizontal velocities

$$U_{\max}(x,y,z) = \sqrt{u^2_{\max}(x,y,z) + v^2_{\max}(x,y,z)}.$$

is presented. Here $u_{\max}(x,y,z)$ and $v_{\max}(x,y,z)$ are amplitudes of the eastward and northward velocities found over one tidal cycle at the position (x,y,z).

Nine horizontal slices of the velocity $U_{\max}$ at depths of between 300 m and 700 m presented in Figure 4 reveal quite a curious tendency. In the surface layers, i.e. shallower than 500 m, the wave energy is mostly concentrated at the periphery of the canyon corresponding to the shelf break area. However, below this depth the regions with high energy concentration are mostly located within the centre of the canyon, not around its edge. This finding is consistent with the observational profiles shown in Figures 3 b and c that reveal the energy maximum at approximately 700 m depth recorded at the CTD station in the middle of the canyon.

Such a focusing of internal wave energy in the canyon's centre can be explained in terms of a superposition of several tidal beams generated at the shelf edge on the periphery of the canyon and radiating downward toward the centre of the canyon, as it is shown in Figure 1 c. Indeed, analysis of the bottom steepness (2) has shown that $\alpha << 1$ in the

surrounding shelf area, but $\alpha > 1$ in the central part of the canyon, see Figure 5. The red zones here, situated along the shelf break, separate the areas of subcritical shelf from the supercritical abyssal part of the canyon.

Figure 5 demonstrates that the main part of the canyon topography is supercritical for semi-diurnal internal tidal waves. As a result, according to theory [*Vlasenko et al.*, 2005], the internal tide in the canyon should take a form of tidal beams generated at the shelf break around the canyon periphery which radiate downward toward the centre of the canyon, as is shown in the scheme depicted in Figure 6. Bearing in mind that the canyon head has a near-circular shape, it is expected that it can function like an optical lens focusing wave energy into its centre. Evidence for that interpretation is presented in Figure 7 a for the vertical cross-section depicted in Figure 2 b by a white line. Three tidal beams can be identified in Figure 7 a (the characteristic lines, equation (1), are shown here by thin white lines). The tidal beam *a*-*b*-*c* is generated at the shelf break point, at *b*, and propagates downward along characteristic line *b*-*c*. The tidal beam wave system, resembling a St.Andrews cross, is generated at the saddle point *e*. The tidal energy propagates from this point along four characteristic lines, *e*-*g*, *e*-*d*, *e*-*h*, and *e*-*f*. It is interesting and relevant to note that the two tidal beams generated at the opposite sides of the canyon, viz. *b*-*c* and *e*-*f* meet in the centre of the canyon in the layer between 600 and 800 m depths which is consistent with the position of the deep-water maxima in vertical displacement, horizontal velocity and shear variance seen in Figures 3 d.

As seen from Figure 5, similar conditions of the energy focusing discussed above, i.e. position of sub-, and supercritical areas, are valid also for many other cross-sections passing through the centre of the canyon. In other words, the tidal energy is converted at

many particular areas around the canyon periphery, and is then radiated towards its centre and accumulated there at the depths of between 500 and 800 m, as is observed in the CTD/LADCP analysis.

Such focusing of wave energy in the canyon's centre should increase the associated level of local water mixing there, since energy cannot accumulate indefinitely. Elevated shear variance is testament to greater elevated mixing at depth (Figure 3 d). As a result of intensified local diapycnal mixing in the centre of the canyon, a quasi stationary density (temperature) gradient is formed across the canyon, as shown in Figure 7 b (the same cross-section as in Figure 7 a). Convergence and divergence of isotherms at the depths of between 500 m to 900 m is clearly seen here from two pairs of isotherms colored in white and magenta. Initially (before the model run) the distance between both (parallel) isolines was equal to 100 m: the upper and lower "white" isotherms were initially at depths of 650 m and 750 m, respectively; the upper and lower "magenta" isotherms were initially at depths of 800 m and 900 m. After ten cycles of tidal action the distance between the two groups of isotherms was modified: at some positions they converged, and at others they diverged. Figure 8 shows the difference between isotherms initially centred at 700 m (Figure 8 a) and at 850 m (Figure 8 b). It is interesting that the convergence and divergence of isolines is opposite for the two depth pairs, Figure 8 a, b.

The formation by diapycnal mixing of quasi-stationary horizontal pressure gradients suggests the existence of geostrophically balanced baroclinic eddies. Quasi-stationary eddy features are clearly seen in Figure 9 in the velocity vectors at depths of 450 m, 600 m and 700 m. The eddy around the topography bank is seen at a depth of 450 m where the tidal beam is still located close to the canyon flank and the shelf edge. However vortical

motions are absent in the centre of the canyon at this depth (450 m). According to the findings presented above, the tidal energy is mostly concentrated beneath 450 m and in the centre of the canyon. Here a baroclinic eddy with cyclonic rotation at 600 m depth and anti-cyclonic rotation at 700 m depth is clearly seen.

To find observational evidence of the predicted baroclinic eddy generated in the middle of the canyon, the following analysis of the LADCP data was performed. First, the barotropic tidal velocities $U_j^{\rm bar}$ and $V_j^{\rm bar}$ were found by averaging of the instant velocity profiles:

$$U_j^{\rm bar} = \frac{1}{H_j}\int_0^{H_j} u_j(z)dz;$$
$$V_j^{\rm bar} = \frac{1}{H_j}\int_0^{H_j} v_j(z)dz.$$

$j = 1, 2, 3, \cdots, 14$. Second, the barotropical tidal signal was removed from the sampling data using the following procedure:

$$u_j^{\rm int} = u_j - U_j^{\rm bar};$$
$$v_j^{\rm int} = v_j - V_j^{\rm bar},$$

The velocity vectors $(u_j^{\rm int}, v_j^{\rm int})$ at depths of 600 m and 750 m along with the model predicted vectors are presented in Figures 10 a and 10 b by black arrows.

It is clear that the remainder baroclinic signal contains both stationary currents and non-stationary internal waves. It is also not free from a random signal that always is present in any observational data set. Note however, that looking at the cluster of velocity vectors as a whole that was recorded in the very same place with one-hour time interval one can discern a consistent pattern. It seems that the general (average) direction of the black arrow clusters in Figures 10 a and 10 b is consistent with that predicted by the model,

i.e. the anti-cyclonic and cyclonic rotation in depths 600 m and 750 m layers, respectively. This can be considered as further evidence that tidal energy focusing in the centre of the canyon is responsible for the formation of baroclinic eddies there.

4. Discussion and conclusions

Submarine canyons are common bathymetric features at many of the world's shelf edge regions. They can trap internal wave energy holding it towards the head of canyons in a converging wave-guide that can lead to a high level of turbulent mixing there. This mechanism was discussed by *Baines* [1983]; *Gardner* [1989]; *Gordon and Marshall* [1976]; *Hotchkiss and Wunsch* [1982]. Note, however, that the aforementioned papers appeal predominantly to a two-dimensional concept of this mechanism. In reality one should operate with three-dimensional characteristic surfaces of a 3D wave equation rather than with the characteristic lines of its 2D counterpart. As a result of the three-dimensionality, the characteristic lines emanating from flanks of a concave topography can focus in its centre producing a spot with high levels of internal wave energy and mixing. This paper deals with the three-dimensional aspects of these effects of the focusing mechanism.

The possibility of intensification of baroclinic tidal energy due to wave interference was recently reported in a number of theoretical papers. *Carter* [2010] analysing model output for baroclinic tide in the Monterey Bay region testified interference of internal waves generated at different sectors of the bay. It was found that the model predicted up to 5 times increase of the baroclinic tidal flux close to the Monterey canyon axis located in the centre of the bay. It was hypothesized there that the effect was created thanks to topographic focusing, although this fact was not clarified, specifically in terms of the beam-like structure of baroclinic tides or supercriticality of the bottom topography.

In fact, the Monterey Bay area is much larger area than just the Monterey Bay canyon. In light of the present study it is important that similar 3D focusing of baroclinic tidal energy, even being mostly theoretically discovered, 1s reported for this and other areas.

Similar effect of the interference of baroclinic tidal energy radiated from scattered multiple sources was also reported by *Rainville et al.* [2010] for the Hawaiian Ridge area. As distinct from the present study, mostly horizontal interference of the baroclinic tidal waves was studied, however the effect of baroclinic tidal energy superposition was clearly demonstrated.

The most recent model study conducted by *Zhang et al.* [2014] for an idealized and supercritical for M_2 tide canyon confirmed an asymmetry of internal tide in the canyon, which presumably is a consequence of the the along-shore effects of propagating internal tidal wave. In fact, they focus mostly on resonant effects of internal tide generation in the canyon, although some details on baroclinic tidal energy focusing are also reported. With relevance to the present study, *Zhang et al.* [2014] reported the beamlike structure of baroclinic tides near the supercritical canyon, with a difference in deepward and shoreward structures, although their interference in the canyon area was not demonstrated

Model output always allows us to study the process of wave focusing in detail, however in reality it is quite difficult to observe this effect in-situ. For the Celtic Sea we have found not only theoretical but also observational evidence of the baroclinic tidal energy focusing in the middle of the canyon. The measurements were conducted during D376 in the centre of the Petite Sole Canyon situated at the shelf edge of the Celtic sea (see Figures 2). CTD and LDCP data collected at a station in the middle of the canyon revealed

large vertical oscillations of isotherms (up to 45 m, Figures 2 b) and local maximum of horizontal currents (up to 0.12 ms^{-1}, Figures 3 c) in the layer between 500 and 800 m.

The possibility of such an inherently three dimensional focusing mechanism of baroclinic tidal energy was confirmed in a series of numerical experiments conducted using the MITgcm forced by M_2 tidal harmonic. The high internal tidal activity in the deep part of the canyon (Figures 4) is treated here in terms of downward propagation and focusing of internal tidal beam generated at the shelf break. The specific circular shape of the canyon, coupled with the steep bottom topography below the shelf break (steeper than tidal beam) in all parts of the canyon create favourable conditions for the tidal energy focusing in the canyon's centre, see Figures 6. Both observations and MITgcm simulations have also shown that the tidal energy focusing intensifies local diapycnal mixing, that can lead to formation of a baroclinic eddy below 450 m depth in the central part of the canyon, see Figures 9. Evidence consistent with the presence of the cyclonic and anti-cyclonic rotation in the canyon centre was found also in in-situ data.

The importance of the results is that the effect of the focussing of baroclinic tidal energy in 3D configuration is quite a typical situation in many areas. This means that the results on the baroclinic tidal energy focusing reported here can have much wider application rather than just circular-shape canyons.

Acknowledgments. This work was supported by the Natural Environment Research Council Grant FASTNEt (award NE/I030259/1). The used data are available at http://www.sams.ac.uk/fastnet.

References

303 Baines, P.G. (1983), Tidal motion in submarine canyons a laboratory experiment, *J. Phys.*
304 *Oceanogr.*, *13*, 310–328.

305 Carter, G.S. (2010), Barotropic and baroclinic M_2 tides in Monterey Bay region, *J. Phys.*
306 *Oceanogr.*, *40*, 1766–1783.

307 Egbert, G.D., and S.Y. Erofeeva (2002) Efficient inverse modeling of barotropic ocean
308 tides, *J. Atmos. Oceanic Technol., 19(2)*, 183–204.

309 Gardner, W.D. (1989), Periodic resuspension in Baltimore Canyon by focusing of internal
310 waves, *J. Geophys. Res.*, *94(C12)*, 18,185–18,194.

311 Gordon, R.L., and N.F. Marshall (1976), Submarine canyons: internal wave traps? *Geoph.*
312 *Res. Let.*, *3(10)*, 622–624.

313 Grimshaw, R.H.J., P.G. Baines, and R.C. Bell (1985), The reflection and difraction of
314 internal waves from the junction of a slit and a half-space, with application to submarine
315 canyons. *Dyn. Atmos. and Oceans*, *9*, 85–120.

316 Hall, R.A., and G.S. Carter (2011), Internal tides in Monterey Submarine Canyon, *J.*
317 *Phys. Oceanogr.*, *41*, 186–204.

318 Hickey, B.M. (1995), Coastal submarine canyons, *Topographic Effects in the Ocean: 'Aha*
319 *Huliko'a Hawaiian Winter Workshop*, Honolulu,HI, University of Hawaii at Manoa,
320 95–110.

321 Hotchkiss, F.S., and C. Wunsch (1982), Internal waves in Hudson Canyon with possible
322 geological implications, *Deep-Sea Res.*, *29(4A)*, 415–442.

323 Jachec, S.M., O.B. Fringer, M.G. Gerritsen, and R.L. Street (2006), Numerical simulation
324 of internal tides and the resulting energetics within Monterey Bay and the surrounding

area. *Geoph. Res. Let.*, *33*, doi:10.1029/2006GL026314.

Kunze, E., L.K. Rosenfeld, G.S. Carter, and M.C.Gregg (2002), Internal waves in Monterey Submarine Canyon, *J. Phys. Oceanogr.*, *32*, 1890–1913.

Pacanowski, R.C., and S.G.H. Philander (1981) Parameterisation of vertical mixing in numerical models of Tropical Oceans. *J. Phys. Oceanogr.*, *11*, 1443-1451.

Petruncio, E.T., L.K. Rosenfeld, and J.D. Paduan (1998), Observations of the internal tide in Monterey Canyon, *J. Phys. Oceanogr.*, *28*, 1873–1903.

Petruncio, E.T., J.D. Paduan and L.K. Rosenfeld (2002), Numerical simulation of the internal tide in a submarine canyon, *Ocean Modell.*, *4*, 221–248.

Polzin, K., E. Kunze, J. Hummon, and E. Firing (2002) The finescale response of lowered ADCP velocity profiles, *J. Atmos. and Oceanic Technol.*, *19*, 205–224.

Rainville, L., T.M.S. Jonston, G.S. Carter, M.A. Merifield, R.Pincel, P.F. Worcester, and B.D. Dushaw (2010), Interference pattern and propagation of the M_2 internal tide south of the Hawaiian Ridge, *J. Phys. Oceanogr.*, *40*, 311–325.

Shepard, F. P. (1974), "Internal waves" advancing along submarine canyons. *Science*, *19*, 195–198.

Thurnherr, A.M., L.C. St.Laurent, K.G. Speer, J.M. Toole and J.R. Ledwell (2005), Mixing associated with sills in a canyon on the Midocean Ridge flank, *J. Phys. Oceanogr.*, *35*, 1370–1381.

Vlasenko V., and N. Stashchuk (2015) Internal tides near the Celtic Sea shelf break: A new look at a well known problem *Deep-Sea Res.*, *103*, 249-36, http://dx.doi.org:10.1016/j.dsr.2015.05.003.

Vlasenko V., N. Stashchuk, and K. Hutter (2005), Baroclinic tides: theoretical modeling and observational evidence. Cambridge University Press. 365 pp.

Vlasenko V., N. Stashchuk, M.Inall, and J.Hopkins (2014), Tidal energy conversion in a global hot spot: on the 3D dynamics of baroclinic tides at the Celtic Sea shelf break, *J. Geophys. Res.*, *119(6)*, 3249–3265, doi:10.1002/2013JC009708.

Wain, D.J., M.C. Gregg, M.H. Alford, R.-C. Lien, R.A. Hall, and G.S. Carter (2013), Prepagation and dissipation of the internal tide in upper Monterey Canyon, *J. Geophys. Res.*, *18*, 4855–4877, doi:10.1002/jgrc.20368.

Zhang,W.Z., T.F. Duda, and I.A. Udovychenkov (2014) Modeling and analysis of internal-tide generation and beamlike onshore propagation in the vicinity of shelfbreeak canyons. *J. Phys. Oceanogr.*, *44*, 834–849.

Zhao,Z., M.H. Alford, R.C. Lien, and M. C. Gregg (2012) Internal tides and mixing in submarine canyon with time-varying stratification. *J. Phys. Oceanogr.*, *42*, 2121–2142.

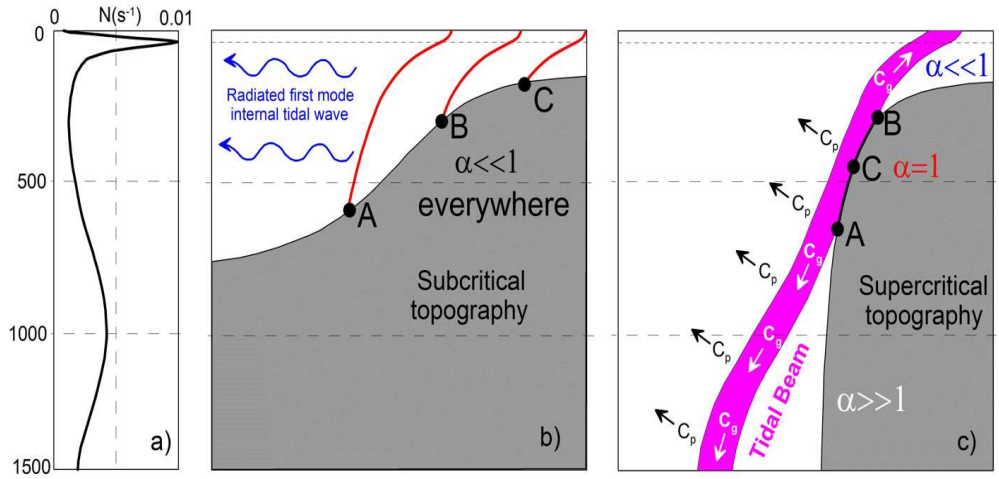

Figure 1. a) Buoyancy frequency measured in the Celtic Sea. b)-c) Schemes of the generation regime over subcritical (b) and supercritical (c) topographies. Red lines in panel (b) show characteristics (1). Magenta area in panel (c) depicts a tidal beam.

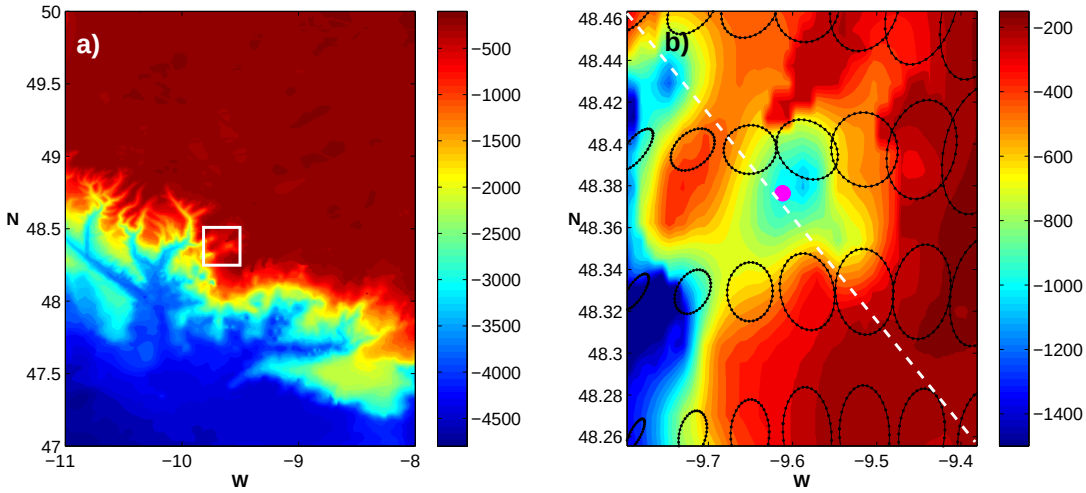

Figure 2. a) Bathymetry of the Celtic Sea. White rectangle shows the position of the canyon. b) Zoom of the Petite Sole Canyon area. The position of the yo-yo CTD station is depicted by a magenta dot. Tidal ellipses showing the intensity of the model forcing are presented by black contours.

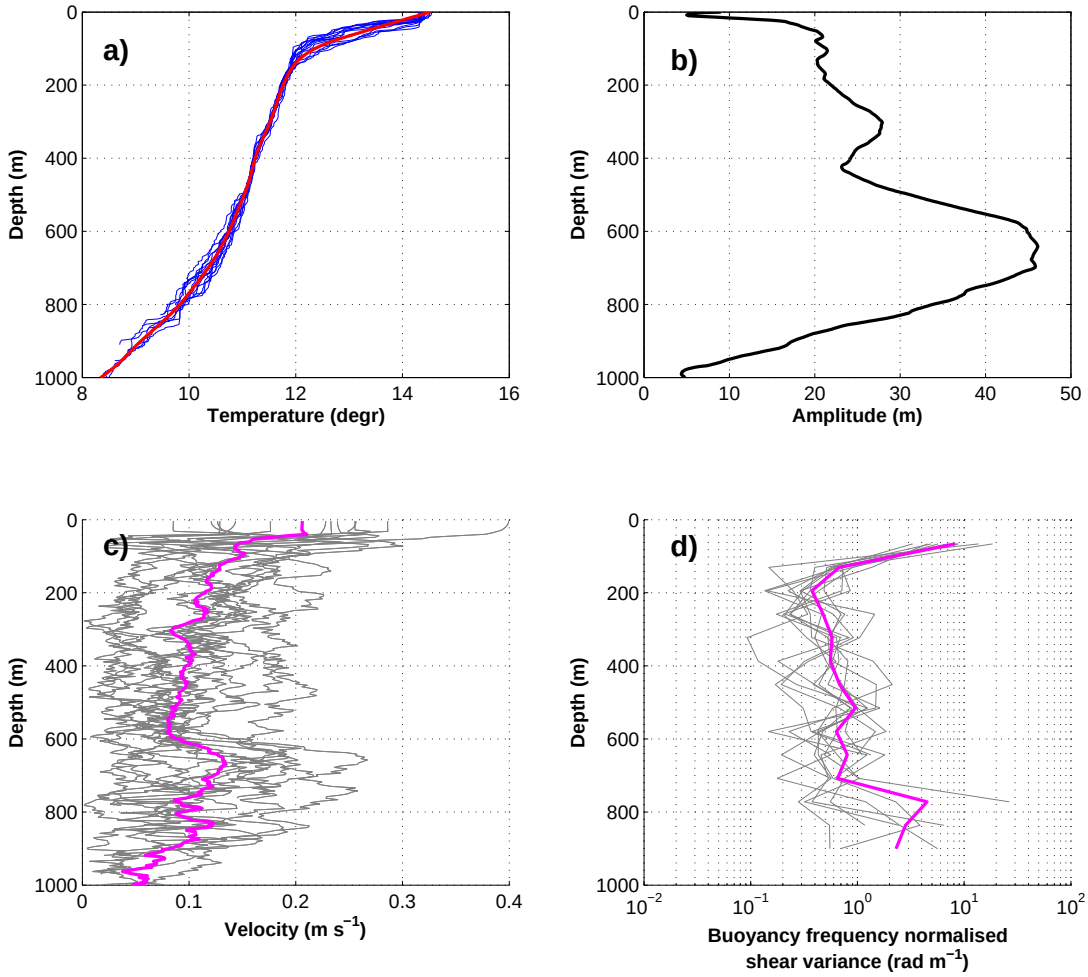

Figure 3. a) Temperature distribution for 14 "yo-yo" CTD mooring (blue lines) with averaged temperature (red line). b) Depth dependant amplitude of temperature deviation. c) Distribution of horizontal velocity from LADCP (grey lines) and mean profile (magenta line). d) Distribution of shear variance, all profiles shown by gray and mean profile with magenta.

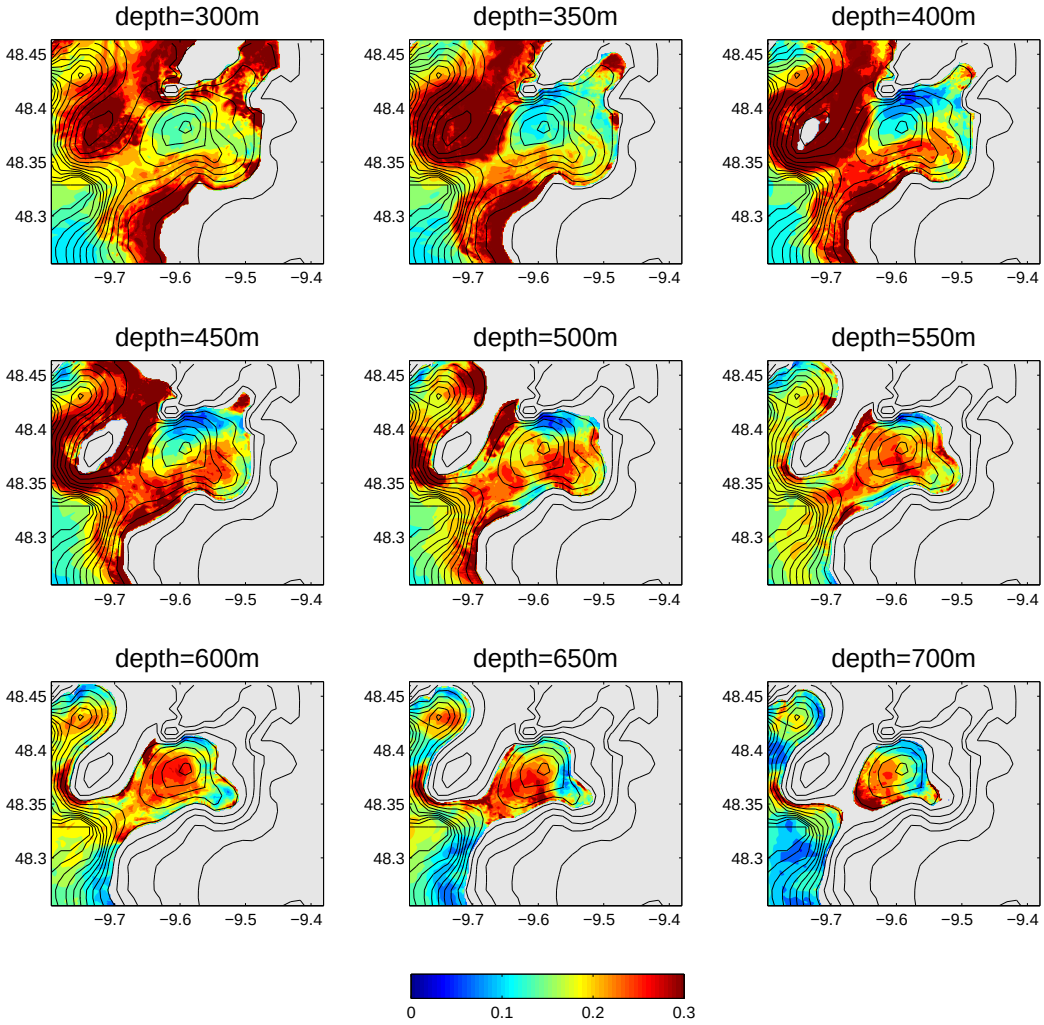

Figure 4. Horizontal distribution of the amplitudes of horizontal velocity at different depths.

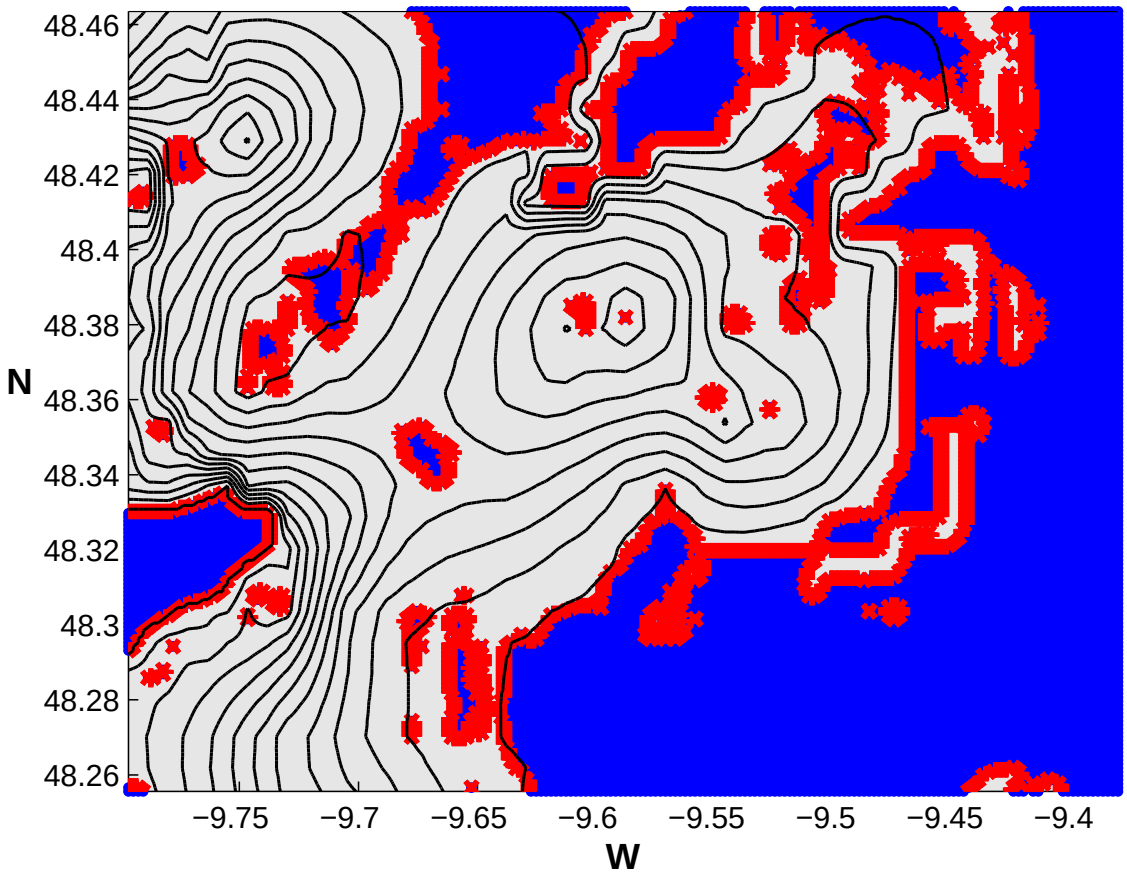

Figure 5. a) Spatial distribution of parameter α: blue areas $\alpha < 1$, red stripes $\alpha = 1$, and clear areas with $\alpha > 1$.

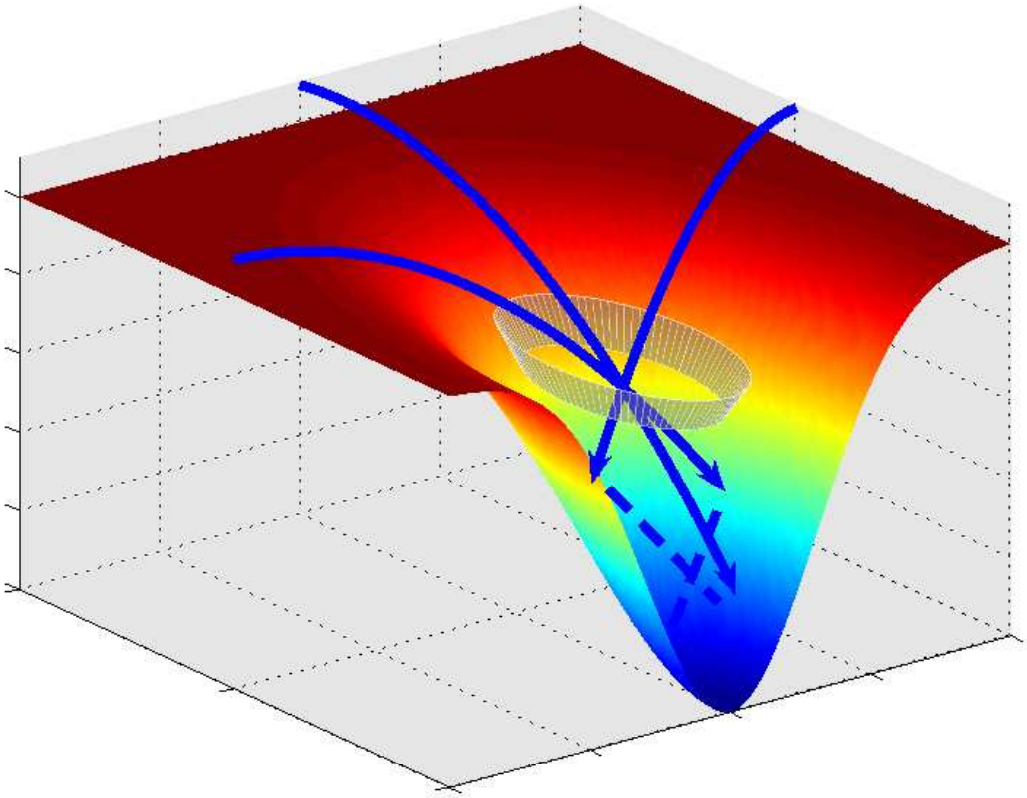

Figure 6. Scheme of intersection of characteristic lines inside idealized canyon and formation of eddy.

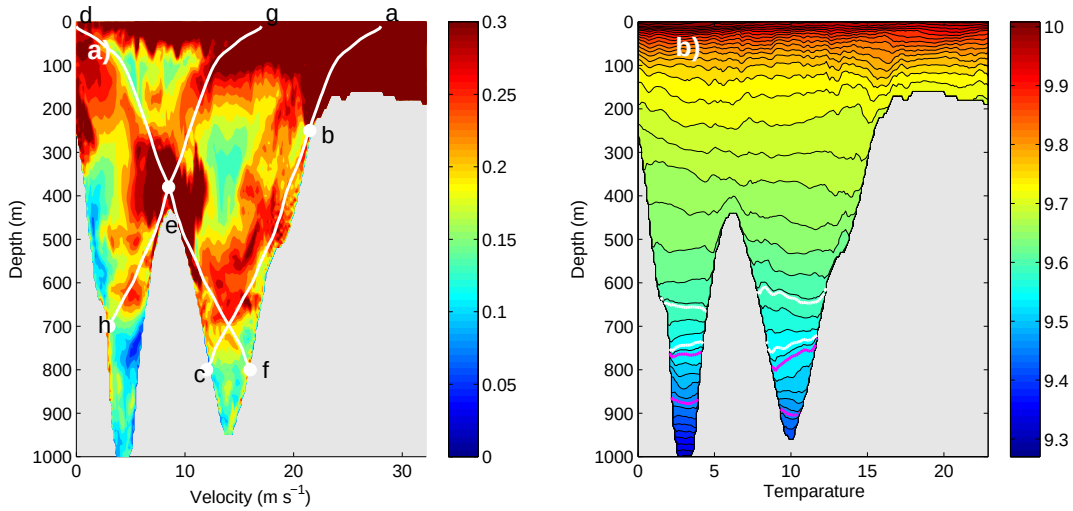

Figure 7. a) The largest values of horizontal velocity and b) averaged temperature distribution along the cross-section (white line in Figure 2 a). The upper white isotherm corresponds to temperature 10.55°C and the lower one to 10.1°C. Similar values for two magenta isolines are 10.0°C and 9.3°C.

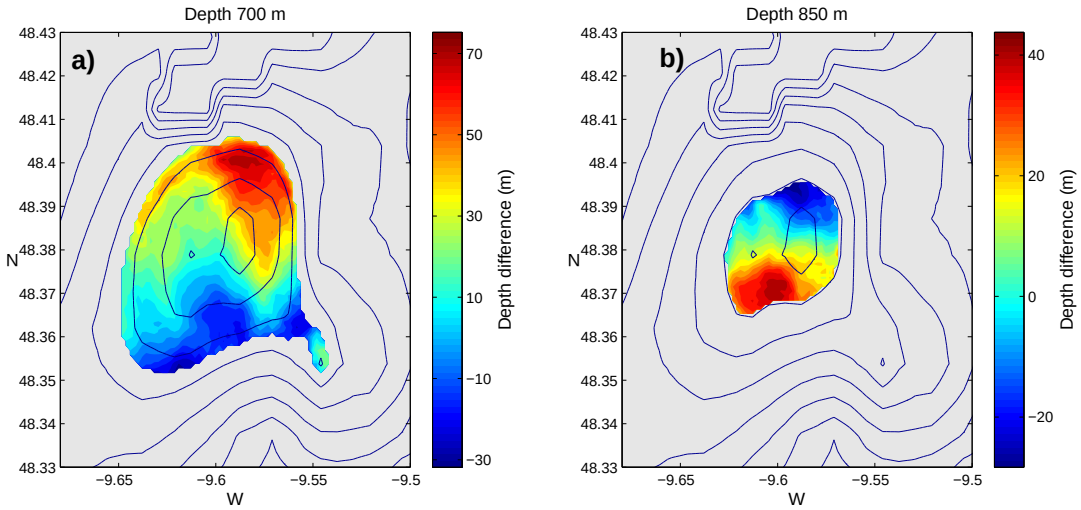

Figure 8. The distance between isotherms shown in Figure 7 b in white (panel a) and in magenta (panel b).

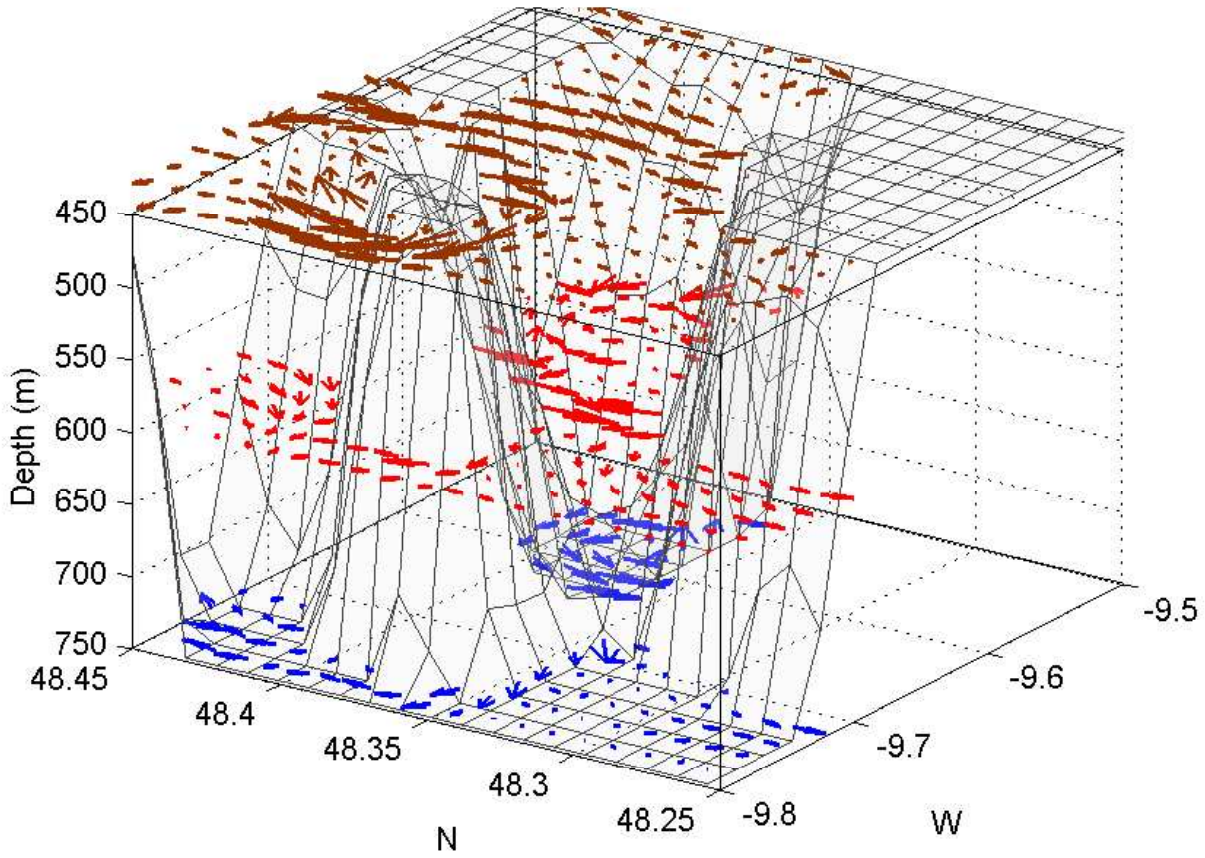

Figure 9. Velocity vectors of the model predicted baroclinic eddy generated inside the canyon.

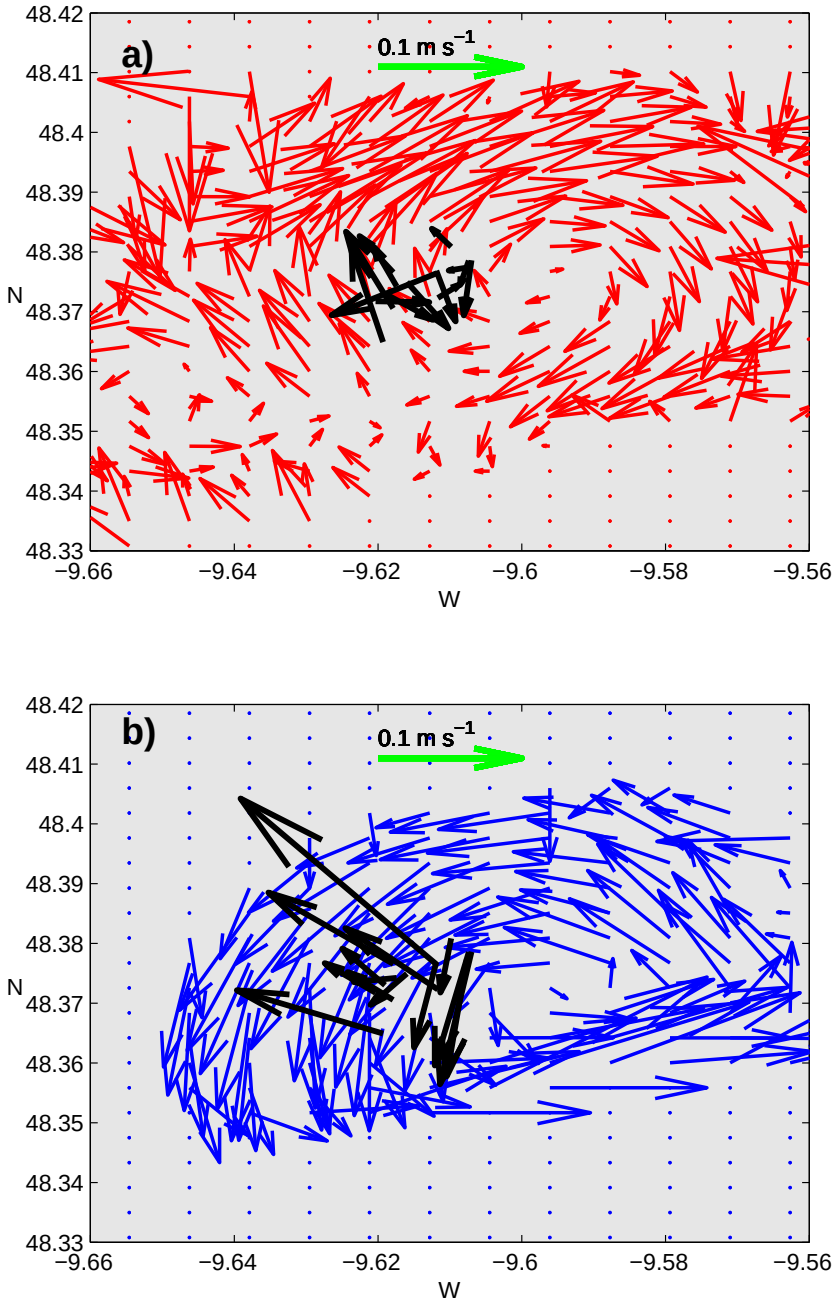

Figure 10. a) and b) Model predicted anti-cyclonic and cyclonic eddies at the depths of 600 m and 750 m (shown by red and blue arrows, respectively). Baroclinic currents recorded by LADCP at 14 "yo-yo" stations at the same depths are shown by black arrows.